ThalesAlenia
A Thales / Finmeccanica Company *Space*

REFERENCE : SD-RP-AI-0629

DATE :   June 09

ISSUE :   01   **PAGE :** 1/35

GALILEO GALILEI (GG)

TECHNICAL REPORT ON SIMULATORS

DRL/DRD: DEL-40

Written by	Responsibility
G. Catastini	Author
Verified by	
n.a.	Checker
Approved by	
	Product Assurance
	Configuration Control
	Design Engineer
	System Engineering Manager
A. Anselmi	Study Manager
Documentation Manager	
R. Cavaglià	

The validations evidence are kept through the documentation management system.

M032-EN

100181547K-EN

ISSUE	DATE	§ CHANGE RECORDS	AUTHOR
01	08-Jun-09	First issue submitted to PRR	

M032-EN

100181547K-EN

TABLE OF CONTENTS

M032-EN

100181547K-EN

1. SCOPE AND PURPOSE

This document is submitted in partial fulfilment of Work Package 1A-ADB of the GG Phase A2 Study (DRL item DEL-40).

The purpose of the document is to provide an overview of the architecture, the design and the use of the software simulators set up during the study to address the complex dynamics of the GG satellite.

2. REFERENCES

2.1 Applicable Documents

[AD 1]   ASI, "Progetto Galileo Galilei-GG Fase A-2, Capitolato Tecnico", DC-IPC-2007-082, Rev. B, 10-10-2007 and applicable documents defined therein

2.2 Standards

[SD 1]   ECSS-M-00-02A, Space Project Management – Tailoring of Space Standards, 25 April 2000

[SD 2]   ECSS-E-ST-10C, Space Engineering - System Engineering General Requirements, 6 March 2009

[SD 3]   ECSS-E-10-02A, Space Engineering – Verification

[SD 4]   ECSS-Q-00A, Space Product Assurance - Policy and Principles, and related Level 2 standards.

2.3 ASI Reference Documents

[RD 1]   GG Phase A Study Report, Nov. 1998, revised Jan. 2000, available at: http://eotvos.dm.unipi.it/nobili/ggweb/phaseA/index.html

[RD 2]   Supplement to GG Phase A Study (GG in sun-synchronous Orbit) "Galileo Galilei-GG": design, requirements, error budget and significance of the ground prototype", A.M. Nobili et al., Physics Letters A 318 (2003) 172–183, available at: http://eotvos.dm.unipi.it/nobili/documents/generalpapers/GG_PLA2003.pdf

[RD 3]   A. Nobili, DEL001: GG Science Requirements, Pisa, September 2008

2.4 GG Phase A2 Study Notes

[RD 4]   SD-RP-AI-0625, GG Final Report / Satellite Detailed Architecture Report, Issue 1

[RD 5]   SD-RP-AI-0626, GG Phase A2 Study Executive Summary, Issue 1

[RD 6]   SD-TN-AI-1163, GG Experiment Concept and Requirements Document, Issue 3

[RD 7]   SD-RP-AI-0620, GG System Performance Report, Issue 2

[RD 8]   SD-TN-AI-1167, GG Mission Requirements Document, Issue 2

[RD 9]   SD-RP-AI-0590, GG System Concept Report (Mission Description Document), Issue 3

[RD 10]   SD-SY-AI-0014, GG System Functional Specification and Preliminary System Technical Specification, Issue 1

[RD 11]   SD-RP-AI-0631, GG Consolidated Mission Description Document, Issue 1

[RD 12]   SD-TN-AI-1168, GG Mission Analysis Report, Issue 2

[RD 13]   DTM, GG Structure Design and Analysis Report, Issue 1

M032-EN

100181547K-EN

[RD 14] SD-RP-AI-0627, GG Thermal Design and Analysis Report, Issue 1

[RD 15] SD-RP-AI-0268, GG System Budgets Report, Issue 1

[RD 16] SD-RP-AI-0621, Technical Report on Drag and Attitude Control, Issue 2

[RD 17] TL25033, Payload Architectures and Trade-Off Report, Issue 3

[RD 18] SD-RP-AI-0629, Technical Report on Simulators, Issue 1

[RD 19] ALTA, FEEP Thruster Design and Accommodation Report, Issue 1

[RD 20] TASI-FI-44/09, Cold Gas Micro Thruster System for Galileo Galilei (GG) Spacecraft - Technical Report, Issue 1, May 2009

[RD 21] SD-RP-AI-0630, Spin Sensor Design, Development and Test Report, Issue 1

[RD 22] SD-TN-AI-1169, GG Launcher Identification and Compatibility Analysis Report, Issue 1

[RD 23] ALTEC-AD-001, GG Ground Segment Architecture and Design Report, Issue 1

[RD 24] SD-TN-AI-1218, GG Preliminary Product Tree, Issue 1

[RD 25] SD-PL-AI-0227, GG System Engineering Plan (SEP), Issue 2

[RD 26] TAS-I, Payload Development and Verification Plan, Issue 1

[RD 27] SD-PL-AI-0228, GG System Verification and Validation Plan, Issue 1

[RD 28] SD-TN-AI-1219, Report on Frequency Management Issues, Issue 1

[RD 29] SD-RP-AI-0632, GG Mission Risk Assessment And Mitigation Strategies Report, Issue 1

[RD 30] SD-RP-AI-0633, Report on Mission Costs Estimates, Issue 1

2.5 External Reference Documents

[RD 31] Any additional references specific to this document are listed here

3. SPACE EXPERIMENT SIMULATOR

3.1 Motivation and Background

Space missions in Fundamental Physics like GG require high precision experiments to be performed in space with no direct access to the apparatus once in orbit. Though this is commonplace for all space missions, space missions at large do not rely on weightlessness as a key feature for the experiment performance. To the contrary, GG as well as other missions in this field (e.g. GP-B, Goce, μScope, Lisa-PF, Step, Lisa …), are designed to perform experiments in absence of weight. Therefore, the experimental apparatus is designed and built to work at zero-g, not at 1-g, and the issue arises as to how effectively such an apparatus can be tested in the lab before launch, and what are the chances for the space mission to perform as expected.

Since flight opportunities are scarce –especially for basic science– and flying a mission, even in Low Earth Orbit, is typically as expensive as large ground projects, it is a must to provide firm evidence before launch that chances to succeed are high.

Considerable effort has been devoted during several years in order to provide strong evidence for the success of the GG mission.

This is done by proceeding along the following three lines:

1. Build up a numerical Space Experiment Simulator of the GG mission in space based on the best know-how available to the most advanced space industries, particularly those with direct expertise in missions which fly zero-g designed payloads

2. Build up a prototype in the lab which is demonstrated to have the key physical features of the payload to fly, and provide experimental evidence that the major requirements of the space mission are met

3. Feed the values of the physical parameters measured in the lab into the Space Experiment Simulator to assess the overall performance of the GG mission.

It is apparent that this is a very challenging plan. Space industry should have the capability required; the payload should have been designed so that a 1-g version of it can be built which maintains its key features; the scientific and industrial teams should be able to work in very close collaboration.

All such conditions are met in GG, in terms of space industry specific know-how, of physical design of the experimental apparatus for it to be significantly tested in the lab, as well as for what concerns a well established tradition of close collaboration between scientists and space industry.

Thales Alenia Space Italy (To) is well equipped to perform the task of building a GG Space Experiment Simulator. In its capacity as prime contractor of the GOCE mission of ESA, TAS-I designed, built, tested and demonstrated the performance of, a complete Space Experiment Simulator for this mission, which has considerable commonalties with GG.

GOCE, launched successfully on March 17th from the Plesetsk cosmodrome in northern Russia, is a very challenging high-tech mission devoted to measuring the gravitational field of the Earth to very high degree and order. It is therefore equipped with very sensitive accelerometers arranged in diamond configuration to accurately measure gravity gradient effects. The accelerometers –designed and built by ONERA (Chatillon, France)– are based on a "free floating" test mass with electrostatics bearing and pick up. Though a tiny mechanical connection is added in order to provide passive electrostatic grounding, the accelerometers as such can work only at zero-g and no full test is possible in the lab. ONERA –with the support of CNES– has indeed already flown similar accelerometers (onboard the Space Shuttle, as well as in previous satellite geodesy missions such as CHAMP and GRACE). However, being the tasks of GOCE more challenging, a Space Experiment Simulator was built by Thales Alenia Space in Torino to check the consistency of spacecraft and payload specifications with the overall system requirements, to support trade-off, sensitivity and worst-case analyses, to support design and pre-validation testing of the Drag-Free and Attitude Control (DFAC) laws, to prepare and test the on-ground and in-flight gradiometer calibration concepts, to prototype the post-processing algorithms, and to validate the performance of the mission. The GOCE simulator has been extensively used during the design and construction of the spacecraft and payload and is the centrepiece of the flight commissioning and calibration activities being carried out at this time.

A delay in the readiness of the launcher has postponed the launch of GOCE by several months, but the satellite is now flying in its low Earth orbit, thus allowing in particular putting the numerical Simulator itself under the most stringent test.

The GG Space Experiment Simulator was initiated –with ASI support– since the first study of the mission, precisely because it was immediately rated as a crucial validating tool. This preliminary simulator allowed the basic physical features of the GG system to be identified and checked; however, it was still too simplified (e.g., it was mostly a 2-dimensional model).

Building up on the expertise acquired with the GOCE Simulator, the GG Space Experiment Simulator could be raised to a very advanced level in the very short time of the GG Phase A2 study. Furthermore, by incorporating in it the physical parameters as experimentally measured in the lab with the Payload Prototype, the accuracy of the simulation was correspondingly enhanced. The combination of (a) flight validation of the orbit and spacecraft environment simulation and (b) lab validation of the experiment parameters, makes the GG simulator an extremely reliable performance validation tool, the like of which was seen in no other similar mission.

3.2 GG Simulator Architecture

The GG simulator solves for the satellite dynamics along an orbit resulting from the application of the Earth's gravity field, the non-conservative environmental disturbances (atmospheric drag, wind, solar radiation pressure, coupling with Earth's magnetic field, etc.) and the DFAC control forces and torques.

The GG simulator is based on three different main modules: the Environment, the Dynamics and the Post-Processing ones. Figure 3-1 shows a description of the GG simulator logical breakdown, highlighting the main data sets exchanged.

The *Environment Module* is in charge of computing the gravity field, the gravity gradient and the non-gravitational forces/torques acting on the spacecraft. These forces and torques are added to the forces of the DFAC and AOCS actuators, in order to realize the GG orbit.
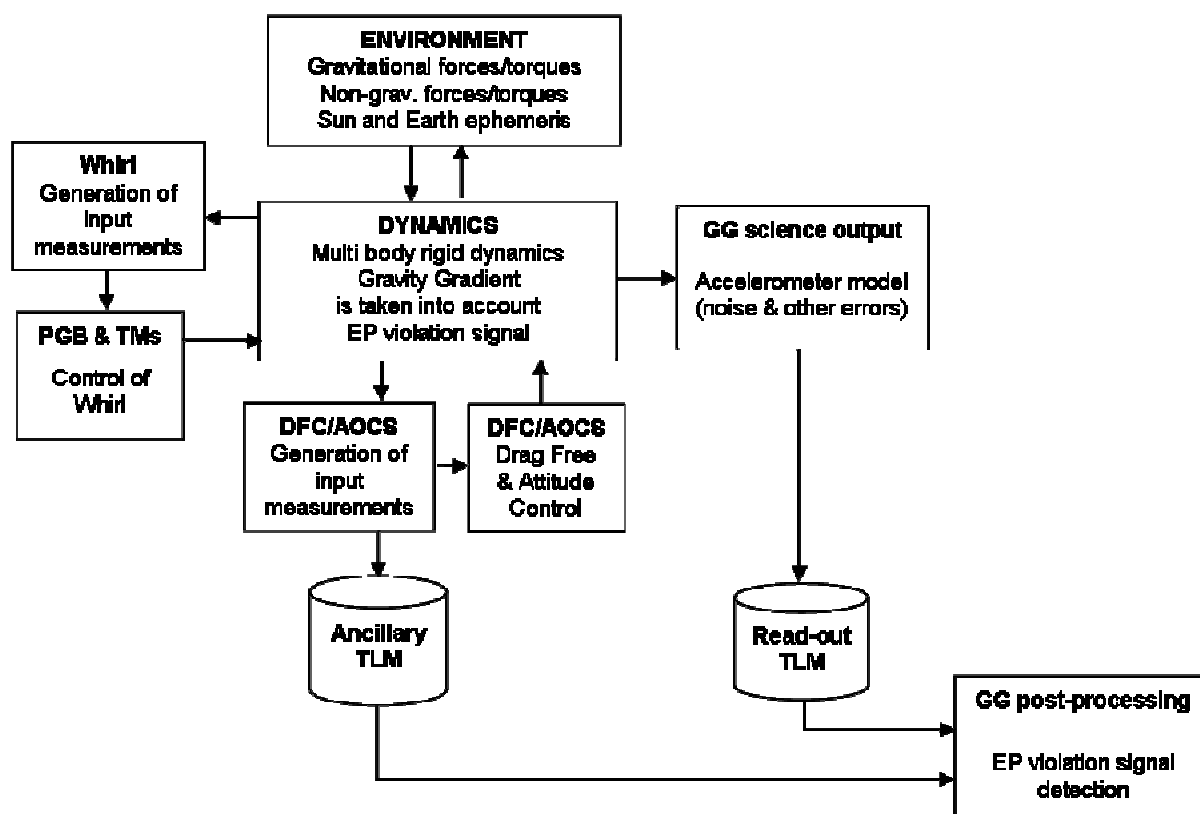

Figure 3-1: GG simulator block-diagram.

The three main modules of the simulator are the Environment, the Dynamics and the Post-Processing modules. The blocks containing the controllers for the damping of the whirling motion of PGB and of the test masses, the Drag Free and the Attitude and Orientation of the satellite are components of the Dynamics module.

M032-EN

100181547K-EN

The *Dynamics Module* is in charge of computing the GG orbit and the relative dynamics of PGB w.r.t. the spacecraft, and of test masses w.r.t. PGB. This module has to take into account the gravity gradient acting on each body inside the GG spacecraft, and of the EP violating signal acting on the test masses. The control laws for the damping of the PGB and test masses whirling motion, for the drag free and the AOCS are also dedicated blocks of the dynamics module. It is also in charge of computing:

- the capacitance measurements used to feed the Whirl control of the PGB and of the test masses (simulation of the capacitance sensors, which feed the whirl controller)

- the forces necessary to damp the PGB and test masses whirl motions (simulation of the actuators, which realise the whirl controller commanded forces)

- the effects due to temperature variations on the inertia properties of spacecraft, PGB and test masses

- the effects due to temperature variations on the mechanical suspension (degrade of the $CMRR_{xy}$ and $CMRR_z$) and on the mechanical balancing of the read-out capacitance bridge

- the effects of the temperature gradients on the mechanical suspension (degrade of the $CMRR_{xy}$ and $CMRR_z$) and on the mechanical balancing of the read-out capacitance bridge

- the DFAC and AOCS sensors' measurements

- the DFAC and AOCS actuators' forces and torques (simulation of the FEEP/cold gas thrusters)

- the ancillary telemetry data and the other spacecraft data

- the GG science output (simulation of the science capacitance sensors measurements, which feed the post-processing module)

The *Post-Processing Module* is a self standing off line post-processor, which is in charge of detecting the EP violating signal in terms of differential test mass displacement starting from the science output (and ancillary telemetry if needed). It is also used to compute accelerations, displacements and other useful vectors in the hereafter defined different reference frames.

3.3 Simulator Reference Frames

The GG simulator describes the satellite orbit w.r.t. the most relevant reference frames for the science mission, which have been also used for the assessment of the Scientific Requirements and of the Error Budget: the Inertial Reference Frame, the Local Vertical Reference Frame and the Body Fixed Reference Frame.

3.3.1 Inertial Reference Frame – IRF –

The fundamental Inertial Reference Frame of the mission is currently realised by the J2000 Equatorial Reference Frame (JERF), which is a Cartesian frame defined as follows (see Figure 3-2):

- Origin, O_{J2000}, located at the centre of the Earth

- X_{J2000} axis at the intersection of the mean ecliptic plane with the mean equatorial plane at the date of 01/01/2000 and pointing positively towards the vernal equinox

- Z_{J2000} axis orthogonal to the mean equatorial plane at the date 01/01/2000

- Y_{J2000} axis completing a right-handed reference frame

The satellite initial conditions (position, velocity and attitude) are defined w.r.t. the Inertial Reference Frame. At t= 0 s, the satellite is lying along the X_{J2000} axis, and its velocity is along the Y_{J2000} one.
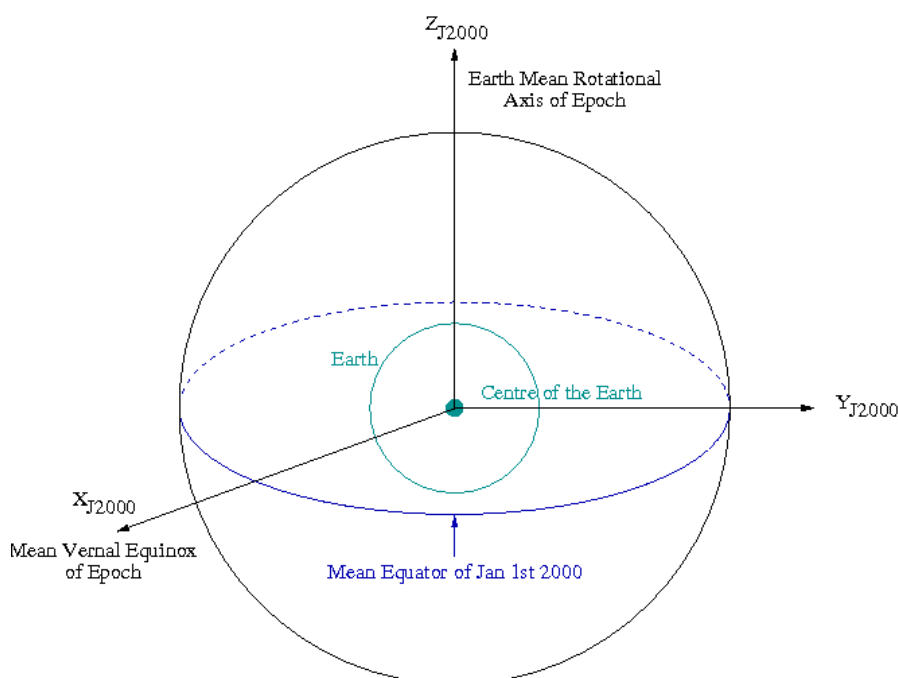

Figure 3-2: The Inertial Reference Frame is the J2000 Equatorial Reference Frame.

The centre is coincident with the Earth centre, the X axis is at the intersection of the mean ecliptic plane with the mean equatorial plane (at the date Jan 1st 2000), the Z axis is perpendicular to the mean equatorial plane (at the date Jan 1st 2000), and the Y axis completes a right-handed reference frame.

3.3.2 Local Vertical Local Horizontal Reference Frame – LVLH –

The LVLH reference frame is the second fundamental frame: in this frame the EP violating signal always appears along a fixed direction (in case of a perfect circular orbit, the Earth is fixed in this reference and the EP violating signal appears as a DC effect). In order to have the EP violating signal along the X_{LVLH} axis, this reference frame is so defined (see Figure 3-3):

- Origin, O_{LVLH}, located at the satellite centre of mass (COM)

- X_{LVLH} axis directed from the centre of mass of the Earth to the satellite centre of mass (X_{LVLH} axis identifies the local vertical from the point of view of the satellite COM)

- Y_{LVLH} axis points toward the direction of motion (it identifies the local horizontal projection of the velocity)

- Z_{LVLH} axis is perpendicular to the orbital plane and completes the right-handed coordinate system.

Notice that because the spacecraft velocity vector rotates, to remain tangential to the orbit, the LVLH system also rotates about the Earth. The LVLH does not take into account the GG spinning about its symmetry axis.

The Post-Processing module of the GG simulator aims to compute the test masses differential displacement due to the EP violating signal w.r.t. the X_{LVLH}, while the main component of the non-gravitational accelerations acting on the spacecraft external surface is along Y_{LVLH}, i.e. 90° out of phase.
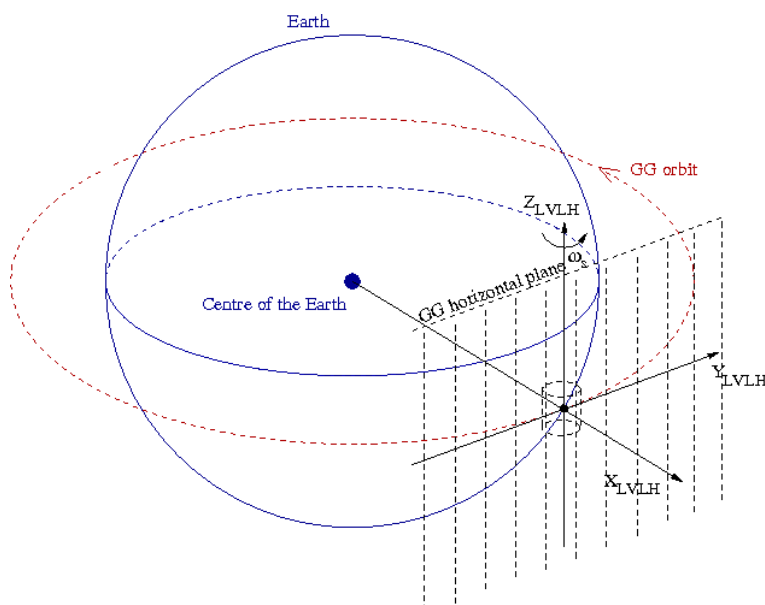

Figure 3-3: The Local Vertical Local Horizontal Reference Frame (LVLH)

The LVLH is a frame co-rotating with the spacecraft. Its origin is coincident with the satellite COM, its X axis is always from the Earth centre of mass to the satellite centre of mass, Y is pointing in the direction of orbit motion (it identifies the local horizontal plane) and its Z axis is perpendicular to the orbital plane and completes the right-handed coordinate system.

3.3.3 Body Fixed Reference Frame – BF –

The Body Fixed Reference Frame is the frame "attached" to the spinning satellite and defined by means of physical markers on the true structure. The necessity of assuming one spacecraft fixed reference frame is dictated by the fact that DFC sensors and actuators are fixed with respect to the satellite structure (PGB and test masses are mechanically suspended and during science operations are not fixed with respect to the satellite structure). The BF frame is defined according to the following prescription:

- The Z_{BF} axis corresponds to the central axis of the PGB connecting cylindrical tube (when the PGB is locked to the satellite). It is nominally the spinning axis of the satellite, and the positive direction is the same of the angular rate vector. In the GG simulator the Z_{BF} axis is the satellite spin axis and it is coincident with the PGB symmetry axis at t=0 s.

- The reference origin, O_{BF}, is located on the Z_{BF} axis. When PGB and test masses are locked with respect to the satellite, the origin marker is placed in order to individuate the position along the Z_{BF} axis of the test masses equatorial plane. O_{BF} is nominally coincident with the satellite centre of mass (when PGB and proof masses are locked). In the GG simulator, O_{BF} is coincident with the satellite centre of mass.

- X_{BF} and Y_{BF} axes lie on the plane containing O_{BF} and perpendicular to the Z_{BF} axis. Each axis passes through the median plane of the two pairs of capacitance plates in between the test masses. A dedicated marker identifies the axes X_{BF} and Y_{BF}, which are chosen to complete with the Z_{BF} axis a right-handed coordinate system. In the GG simulator, it is assumed that the capacitance plates defining the X_{BF} axis are the ones on the X_{J2000} at t = 0.

3.4 Simulator Environment Module

This block is dedicated to the computation of the forces and torques acting on the spacecraft and resulting from the interaction with the orbital environment. As such, this module computes the gravity force, the gravity gradient torque, the aerodynamic force and torques, the magnetic torque, the solar radiation pressure force and torque. It includes:

- the Earth gravity field, with gravitational constant GM = $3.986004418 \cdot 1014$ m^3/s^2, according to the EGM96 Earth Gravity field solution, and Earth Mean Radius = 6378144 m. The gravity gradient torque taking into account for J2 effect is also applied on each body.

- the MSIS86 atmospheric model for the computation of the air density, temperature and chemical composition along the satellite orbit. The F10 and F10.B indexes related to the Solar activity and the Geomagnetic indexes Ap and Kp are used to feed the MSIS model.

- a model of the Earth's magnetic field derived from the Oersted satellite measurements

- the celestial bodies ephemeredes computation

The solar radiation pressure and Earth albedo are computed modeling the satellite surface as a set of one cylinder and two simple flat surfaces. The pressures due to the solar and Earth albedo, which depend mainly on the distance from the Sun, on the altitude of the satellite during its orbit, and on the angle between the Sun direction and the local-vertical direction, is computed for each elementary surface. Once the pressures have been computed, the corresponding forces for each surface are obtained considering the normal and tangent components depending on the surface extension and on the aspect angle of the surface with respect to fluxes direction. The force is computed for each surface and applied to the surface's centre of pressure. The resulting force and torque on the centre of mass of each body is then computed.

3.5 Simulator Dynamics Module

The complete GG system, which takes into account the spacecraft, the Pico Gravity Box, the inner and outer test masses, has been simulated by using the DCAP (Dynamics and Control Analysis Package) software package developed by Thales Alenia Space under ESA contract. An additional dummy body has been introduced in order to solve for the orbit without introducing numerical errors due to the high spinning frequency of the spacecraft itself (the orbit is solved in the reference frame of the first body of the kinematics chain). The dummy body is a massive point coincident with the spacecraft centre of mass: its motion w.r.t. the Inertial Reference Frame is defined by the degrees of freedom (3) of the Hinge 1, which connects it (Node 1) to the origin of the IRF. Moreover, the dummy body identifies the origin of the LVLH reference frame: the vector pointing towards the Earth identifies the X-axis, its velocity identifies the Y-axis (along-track direction), and the orbit angular velocity is along the Z-axis. The bodies are characterized by the up-to-date values of the mass and inertia properties, while the dummy body – Body 1 - is a unitary massive point coincident with the spacecraft centre of mass (Node 10). The bodies of the GG dynamical model (schematically represented in Figure 3-4) and the degrees of freedom (summarised in Table 3-1) are defined as follows:

- Body 1 is the dummy body. Its representative node (Node 1) is coincident with the spacecraft centre of mass. The Hinge 1, which connects the IRF to Node 1, has 3 degrees of freedom: its translation completely describes the orbit motion of the spacecraft.

- Body 2 is the spacecraft. The satellite has its centre of mass (Node 10) coincident with the dummy body (Node 1). The null-length Hinge 2, which connects the LVLH origin to the s/c centre of mass, permits satellite rotations only. In particular, the rotation about the Z axis defines the spin w.r.t. the LVLH.

- Body 3 is the Pico-Gravity Box (PGB). The Hinge 3, which connects the s/c centre of mass (Node 10) to the PGB centre of mass (Node 20), provides the 6 degrees of freedom (3 rotations and 3 translations) of the PGB-s/c relative motion.

- Body 4 is the outer (external) test mass (TMe). The Hinge 4, which connects the PGB centre of mass (Node 20) to the TMe centre of mass (Node 30), provides the 6 degrees of freedom (3 rotations and 3 translations) of the TMe-PGB relative motion.

M032-EN

100181547K-EN

- Body 5 is the inner test mass (TMi). The Hinge 5, which connects the PGB centre of mass (Node 20) to the TMi centre of mass (Node 40), provides the 6 degrees of freedom (3 rotations and 3 translations) of the TMi-PGB relative motion.

This type of multi-body connection grants an open-loop kinematics topology, with no need for cut-joint hinges. All hinges are described by a Euler sequence Type 1, x-y-z. The active degrees of freedom (DoF) defined by hinges can be differently set depending on the required type of simulation.

Hinge Id.	Transl. Dofs (x,y,z)	Rotational Dofs (x,y,z)
1	F, F, F	L, L, L
2	L, L, L	F, F, F
3÷5	F, F, F	F, F, F
Note : L = Hinge DoF Locked F = Hinge DoF Free		

Table 3-1: Translation and rotational degrees of freedom of the hinges defining the kinematics chain of the GG system. Hinge 1 connects the IRF to the dummy body, and the null-length Hinge 2 connects the dummy body to the spacecraft centre of mass.

The Hinge 1 defines also the initial condition for the GG orbit (w.r.t. the IRF), with the convention that at t = 0 the satellite position is ($R_\oplus$ + h, 0, 0) and the satellite velocity is (0, v_y, 0), with $R_\oplus$ the Earth equatorial radius and h the GG orbit altitude. The Hinge 2 defines instead the satellite spin w.r.t. the IRF: initially it has been assumed to be 2 Hz, but it is going to be updated to 1 Hz, according to the last analyses, which have been performed in order to verify the capability of FEEPs and cold gas thrusters for the drag free compensation.

The mass and inertia properties used in the simulator have been fixed at the beginning according to the last Phase A Report description (2000); then, they have been updated according to the March review mass budget. At the end they shall be updated according to the last mass budget. The mass and inertia properties are not continuously updated in order to make more efficient the "growth" of the simulator (the main job is adding all the possible spurious effect masking or competing with the EP signal).
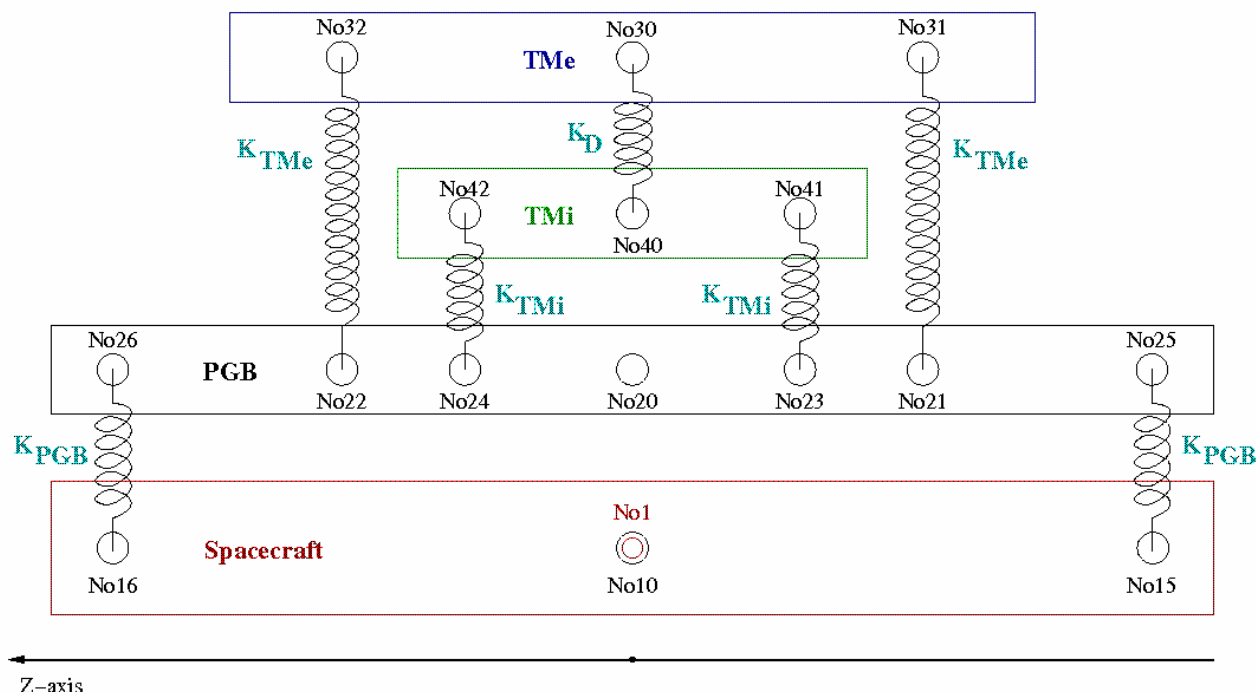
Figure 3-4: Schematic model of the GG dynamics system.

Logical scheme of the dynamical model implemented within DCAP software code for finite element simulation of the space experiment. The z axis is the spin/symmetry axis of the system; all elastic connections along z are very stiff; the plane of sensitivity is perpendicular to z. The model encompasses all bodies (spacecraft, PGB and 2 test masses), each one with its 6 degrees of freedom in 3D (3 for translation and 3 for rotation), mass and moments of inertia. All non rigid components of the system (sketched as springs) are implemented with their designed stiffness (in the sensitive plane as well as in the z direction) and mechanical quality factors Q for simulation.

The mechanical suspensions connecting the PGB to the spacecraft and the test masses to the PGB, which are schematically represented by springs in Figure 3-4, are implemented in order to provide realistic suspension modes (according to the GG on the Ground measured values) and transfer function (see Table 3-2). The PGB-s/c suspension is also characterised by its realistic dissipative term, corresponding to a mechanical quality factor $Q_{PGB} \cong 90$, in order to provide the most realistic representation of the PGB-s/c dynamics behaviour: the PGB-s/c relative motion not only must be measured in order to feed its control of the whirl motion, but provides also the input of the DFAC control, which is a key point for the GG science performance.

GG sub-system	Planar oscillation period [s]	Axial oscillation period [s]
s/c-PGB	360	30
PGB-TMe	$30 < T_{CMxy} < 120$	30
PGB-TMi	$30 < T_{CMxy} < 120$	30
TMe-TMi	540	0

Table 3-2: Oscillation periods of the various GG subsystems along the satellite spin axis and in the plane perpendicular to it.

The dissipation of the PGB-test masses suspensions is instead assumed to be greater and greater than the true one, by adopting a corresponding mechanical quality factor $Q_{TM} \cong 500$ (vs. a true value of $Q_{TM} \cong 20000$): this choice is necessary in order to have a whirl-radius doubling time t_{rw2} of the order of $t_{rw2} \approx 10000$ sec (vs. a true value of $t_{rw2} \approx 500000$ sec). This shorter t_{rw2} permits to carry out simulations covering a mission time duration not longer than $200000 \div 300000$ sec, but which cover all the relevant aspects in terms of disturbing effects and science performance (the EP signal is in fact detected). The adoption of the true value for the mechanical quality factor of the PGB-test masses suspension would force the length of one science performance simulation to several millions of seconds, just to verify the growth of the whirling motion! It is apparent that there is nor loss of generality, neither a "favourable" assumption in this choice.

The EP violating signal is simulated with a force with amplitude $F_{EP} = m_{TM} \cdot g(h) \cdot \eta$ N, which is directed from the Earth centre of mass to the centre of mass of the outer test body only (it is a pure differential force for the test masses). This mean that the EP violating force is always directed along the X_{LVLH} axis. The mass of the proof body is 10 kg, the value of the local gravity sensed from the test mass depends on the GG altitude, and it is about $8 \div 8.4$ m/s^2. The Eötvös parameter η is an input value for the simulator, with η in the range of $10^{-17} \div 10^{-13}$.

High-fidelity models represent sensors feeding the control algorithms and the actuators (FEEPs/cold gas thrusters and spinning-up gas thrusters), which are in charge of generating the DFAC and AOCS commanded forces and torques. The high-fidelity models for sensor and actuators have to account for intrinsic noises, transfer functions, non linearity, mounting errors, sensor/actuators inner geometrical imperfections (see Figure 3-5), temperature fluctuations, quantization and all the other effects which can degrade the scientific performance of the sensors/actuators, since the goal of the simulation is predicting the realistic mission scientific performance.
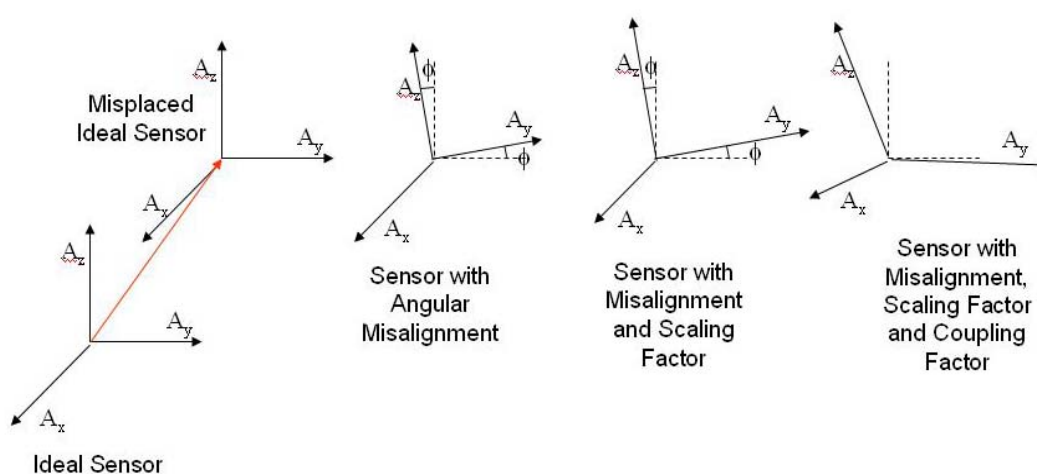

Figure 3-5: Sensor/actuator geometrical imperfection: mispositioning, misalignment, scale factor error and coupling error.

The simulation of sensor/actuator noise and of temperature fluctuation is based on the superposition of deterministic noise (implemented by sinusoidal terms) and of stochastic noise (implemented by noise shaping technique). With the noise shaping technique, a properly devised (in the frequency domain) noise shaping filter is used to provide the desired shape to its feeding unitary band limited white noise. The block-diagram of the white noise shaping technique is reported in Figure 3-6: a unitary (one-sided) white noise is passed through an analog/digital filter that builds up the requested noise Spectral Density and which integrates also an anti-aliasing filter (if necessary). The output of the filter is then decimated (if requested) and saved into a dedicated variable.
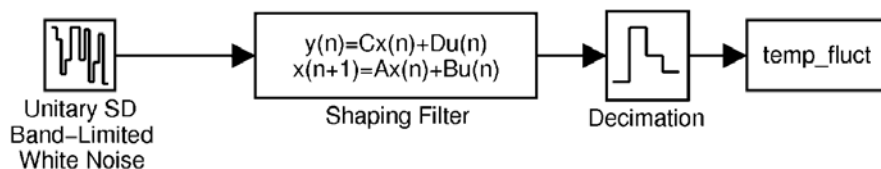
M032-EN

100181547K-EN

Figure 3-6: Block diagram of the white noise shaping technique. A white noise with unitary (one-sided) Spectral Density is passed through a shaping filter (applying also the anti-aliasing, if necessary) and decimated (if required) before saving the output into a dedicated variable.

Figure 3-7 shows as example the time histories of the fluctuating temperature, temp_fluct, realized according to the white noise shaping technique. Figure 3-8 shows the Spectral Density (SD) as computed from the simulated time history, vs the desired analytic SD: the desired analytic SD can be superimposed to the computed one.
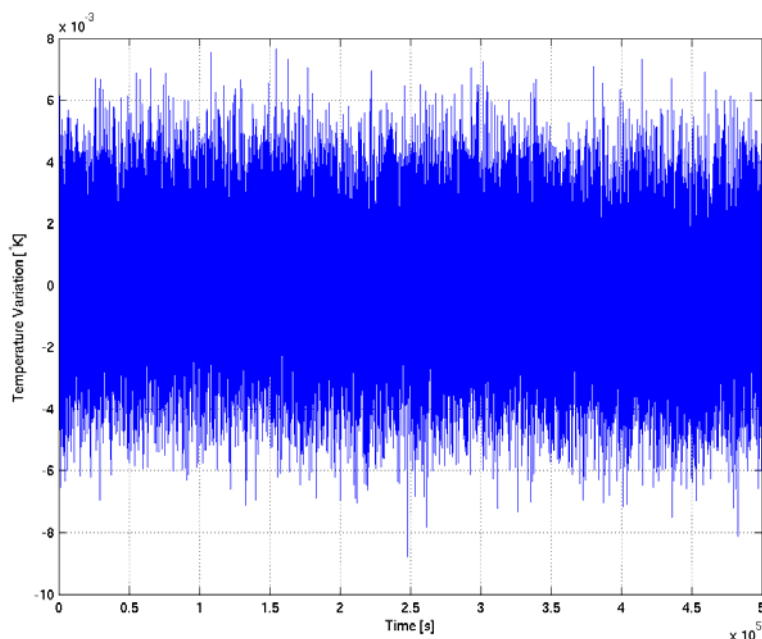

Figure 3-7: Time history of the fluctuating component of temperature obtained with the white noise shaping technique
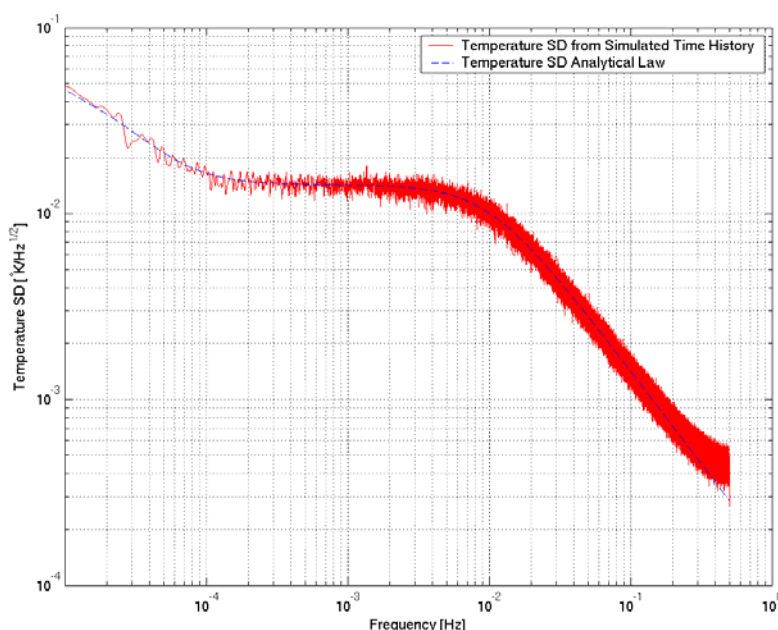
M032-EN

100181547K-EN

Figure 3-8: Spectral density of the temperature fluctuation computed from the simulated time history vs. the Spectral density desired analitic law.

The above cited technique provides the capability of adding the temperature effects sensed at the level of the test masses (thermal noise, temperature fluctuation), of the mechanical balancing of the science read-out, and of the $CMRR_{xy}$ and $CMRR_z$ variation due to temperature.

An analytic function for the temperature variation sensed from spacecraft and PGB shall be instead modelled in order to introduce their inertia variations.

The simulator architecture allows easy incorporation of models generated by a wide range of software tools, such as DCAP-RT (Dynamics and Control Analysis Package for Real Time, TAS-I developed dynamics package), and commercial off the shelf tools like Matlab/Simulink and Real Time Workshop.

3.6 Post-Processing Module

The GG sensor and actuators are fixed w.r.t. the spinning satellite: this means that the detection of the EP violation signal and of the other interesting information (non-gravitational acceleration, whirling motion, temperature effects, gravity gradient contributions, etc.) is completely masked by the GG spinning frequency.

The Post-Processing module, which is in embryonic status (Phase A level), consists of a Matlab macros package, which has been implemented in order to allow the transformation of all the sensor measurements from the BF to the IRF and to the LVLH reference frames. Also the ancillary information about the satellite, PGB and test masses dynamics is provided in all the reference frames, in order to allow the science performance check by using the time histories generated by the simulator. The implemented macro package requires the Signal Processing

and Statistics Matlab Toolboxes. The coding of this module is such that it should be easy a full porting to the GNU Octave environment, which is a free Matlab clone providing also packages equivalent to the Signal Processing and Statistics Toolboxes.

The Post-Processing module allows the analysis on both the time and frequency domain, providing results in terms of Amplitude Spectrum and Spectral Density of the interesting signals (e.g. Fourier analysis of the non-gravitational accelerations w.r.t to IRF and Spectral Density accelerations and displacements).

A further development of this module is foreseen in case of advance in Phase B of the GG science mission.

M032-EN

100181547K-EN

REFERENCE : SD-RP-AI-0629

DATE :   June 09

ISSUE :   01   **PAGE :** 22/35

4. SCIENCE PERFORMANCE SIMULATION

The results of one science performance simulation are hereafter reported in order to validate the GG simulator and to show its capabilities and usefulness. This simulation was carried out in order to check the real basis of the experiment, i.e. the capability to detect the EP violating signal, taking into account:

- the gravity field and the gravity gradient acting on the spacecraft

- the non gravitational forces acting on the spacecraft surface

- the dissipation of the mechanical suspensions (whirling motions and whirl controls of PGB and test masses)

- the gravity gradient acting on the proof masses.

For this exercise, the sensors' and actuators' noise and imperfections have been neglected, in order to compare the simulator's results vs. the analytical predictions. Moreover, it is assumed a perfect Common Mode Rejection Ratio of the mechanical suspensions ($\chi_{CMRRxy} = 0$, $\chi_{CMRRz} = 0$), and a perfect mechanical balancing of the science capacitance bridge ($\chi_{bridge} = 0$). Due to the perfect rejection of the common mode by means of the mechanical suspension, the DFC for the partial compensation of the non-gravitational disturbances is not working in this simulation. The satellite spin frequency has been updated to the new default value: 1 Hz. For this exercise the oscillation periods of the test masses and of PGB have been modified (compare Table 4-1 vs. Table 3-2) in order to largely amplify the displacements due to the inertial acceleration sensed by the bodies (this is due to the fact that the adopted environment cannot be considered a worst case scenario).

GG sub-system	Values of simulated Planar oscillation period [s]	Values of simulated axial oscillation period [s]
s/c-PGB	295.04	295.04
PGB-TMe	$T_{CMxy} = 113$	113
PGB-TMi	$T_{CMxy} < 113$	113
TMe-TMi	500	0

Table 4-1: Oscillation periods of the various GG subsystem along the satellite spin axis and in the plane perpendicular to it adopted for this science performance simulation.

THALES

M032-EN

100181547K-EN

The orbit altitude for this simulation has been chosen to be 520 km, which is not the reference altitude of the science mission, but the one for which the local gravity is 8.4 m/s^2: this value of local gravity was the driver for the EP violating signal for this simulator run. The implemented EP violating signal is the minimum detectable one, i.e. it is due to $\eta=10^{-17}$. Such a signal is simulated with a force with amplitude $F_{EP} = m_{TM} \cdot g(h) \cdot \eta = 8.4 \cdot 10^{-16}$ N, always directed along X_{LVLH} and acting on the outer test mass only. The initial time for the orbit has been assumed to be 2013 July 7th, 6 a.m.: the solar radiation indexes used for this simulation are F10 = F10.B = 120, the geomagnetic index is 8: Figure 4-1 shows the GG orbit and the initial conditions of the simulation (satellite on the X_{IRF} axis). The solar radiation pressure has been taken also into account. The spacecraft area to mass ratio used for the simulation is 0.0032 m^2/kg, which is slightly better than the up-to-date true one (0.005 m^2/kg), but still representative.
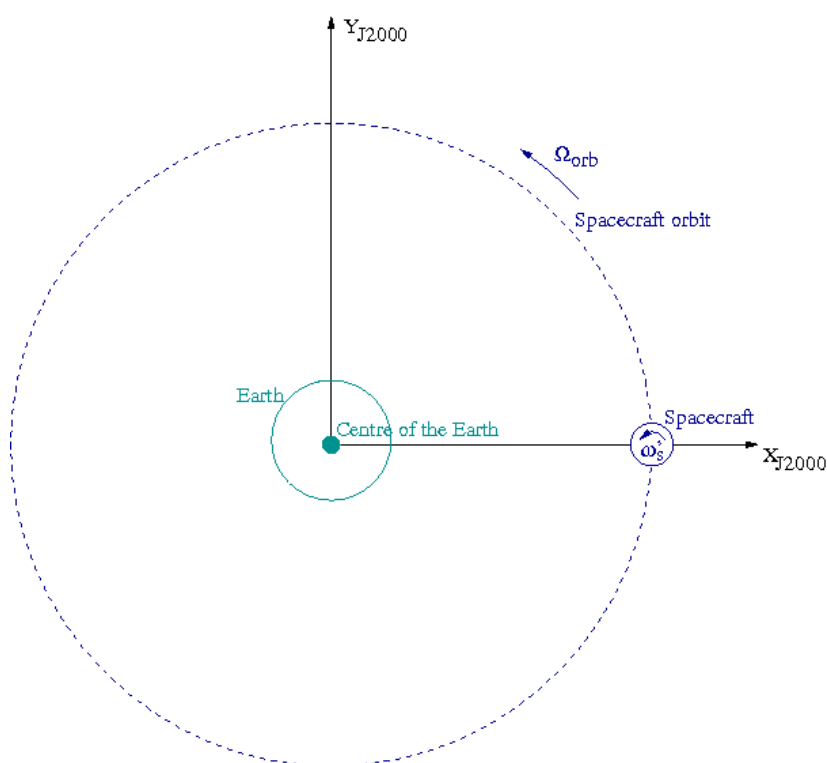

Figure 4-1: Scheme of the initial conditions for the satellite orbit of this simulation.

At t = 0 Hinge 1 locates the satellite w.r.t. the IRF with the position vector r = (R$_\oplus$ + h, 0, 0), with R$_\oplus$ the Earth equatorial radius and h the GG orbit altitude. The satellite velocity is so v = (0, v$_y$, 0).

The continuous controllers of the whirling motion of the PGB and test masses are fed by ideal capacitance sensors and realized through ideal capacitance actuators.

4.1 Satellite acceleration in the LVLH reference frame

One of the main features of the simulator is the capability to compare the accelerations that have to be compensated/rejected and the acceleration that has to be detected: the non gravitational forces acting on the external surface of the spacecraft provides an inertial acceleration that is several orders of magnitude bigger than the EP violating signal. The LVLH components of the spacecraft non gravitational acceleration have been computed by using the Post-Processing module and shown in Figure 4-2, Figure 4-3 and Figure 4-4 below.

Figure 4-4, which shows a zoom of the time histories of the spacecraft acceleration along the Z_{LVLH} axis, highlights also the oscillating term due to the mechanical coupling with the PGB. It has to be pointed out here that the realized simulation is not yet the worst case scenario for the environment, and that it is just one possible representation for the satellite dynamics. The worst case scenario for the environment shall be taken into account once the satellite configuration and the possible launch date will be frozen. The short eclipse periods are also visible: during the eclipse the mean value of acceleration is zero.
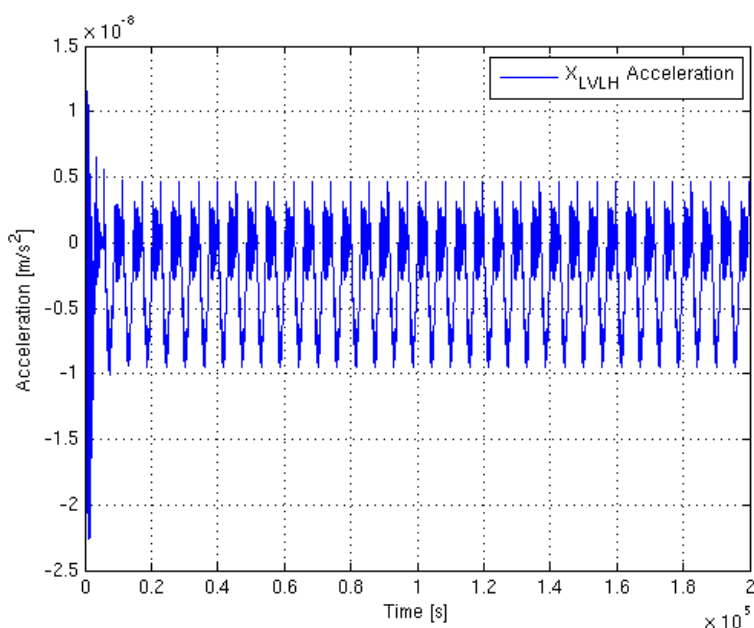

Figure 4-2: Time history of the spacecraft non gravitational acceleration along the X_{LVLH} axis, i.e. along the same direction of the EP violating signal, whose amplitude is $8.4 \cdot 10^{-17}$ m/s^2.
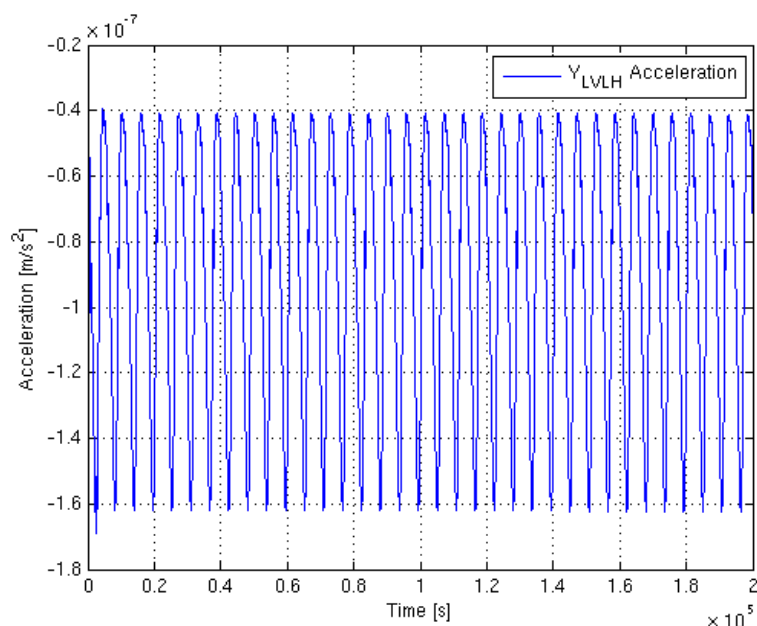
Figure 4-3: Time history of the spacecraft non gravitational acceleration along the Y_{LVLH} axis, i.e. perpendicular to the direction of the EP violating signal, whose amplitude is $8.4 \cdot 10^{-17}$ m/s^2.
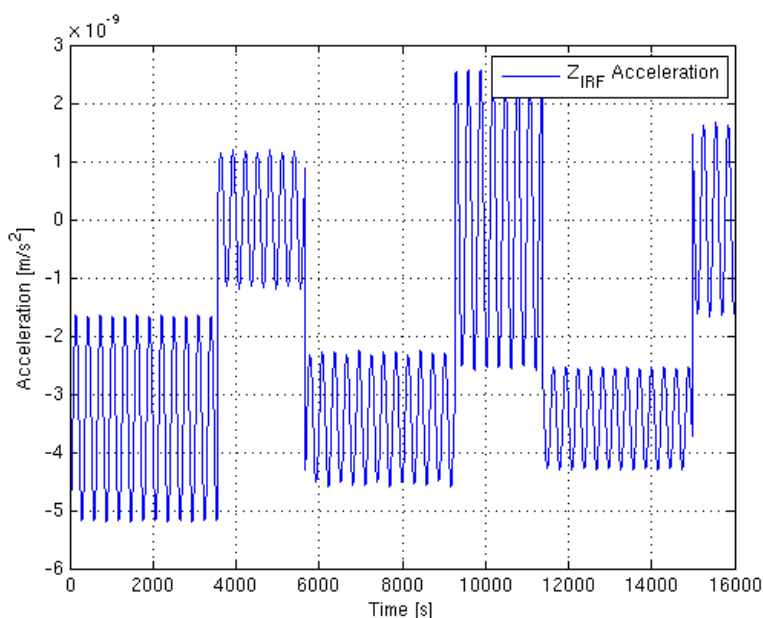

Figure 4-4: Time history of the satellite non gravitational acceleration along Z_{IRF}

Zoom of the time history of the satellite non gravitational acceleration along the Z_{IRF} axis (Z_{LVLH} is parallel to it, there is only translation of the origin), i.e. perpendicular to the orbit plane. The relative motion of PGB w.r.t. the spacecraft is represented by the oscillations of the signal. The short eclipse periods are also visible (acceleration mean value is zero).

4.2 PGB-s/c displacement

The PGB-s/c displacement is analyzed in the Drag Free control document [RD 16].

4.3 Common mode motion of the test masses

The displacement of each test mass w.r.t. the PGB provides the information about the required overall rejection of the common mode acceleration. The overall external non-gravitational force affecting the spacecraft motion is sensed from the test masses as inertial force: in principle it is a pure common mode for them, such as in this simulation. In true life, it is anyway necessary to reduce this common mode acceleration for mainly three reasons:

- the common mode acceleration displaces each test mass, and this displacement has a limited range: the gap of the science capacitance plates

- the common mode rejection of the test masses mechanical suspension is not 0 (i.e. a fraction of the common mode acceleration is transformed into differential acceleration, which competes with the interesting signal to be detected)

- the capacitance read-out, which is in charge of detecting the test masses relative displacement due to an EP violation, is sensitive to both common and differential mode. Hence (a) Its dynamic range must be not saturated; (b) Its rejection of the common mode is limited.

In order to have a very small gap for the capacitance plates of the science read-out (i.e. high sensitivity), the external non-gravitational acceleration is partially compensated by means of an active Drag Free Control, which reduces the inertial acceleration sensed from the PGB and test masses at the orbit frequency. The remaining common mode acceleration is rejected from the mechanical suspension. In the IRF, the residual common mode acceleration sensed from the PGB and test masses at the orbit frequency is $a_{CMxy} = \chi_{DFCxy} \times a_{NGxy}^{ext}$. The a_{CMxy} acceleration is responsible of the elongation of the "springs" connecting the PGB to the spacecraft and the test masses to the PGB in the test masses equatorial plane XY.

In this simulation, whose main objective is the simulator validation, $\chi_{DFCxy} = 1$ (no DFC) and so $a_{CMxy} = a_{NGxy}^{ext}$. The inertial acceleration, which becomes a differential term due to the mechanical balance suspension imperfections, is $a_{DM}^{iner} = a_{CMxy} \times \chi_{CMRRxy}$, wih χ_{CMRRxy} the suspension Common Mode Rejection Ratio. As already mentioned above, in this simulation $\chi_{CMRRxy} = 0$, instead of $\chi_{CMRRxy} = 10^{-5}$ (perfect common mode rejection): so, $a_{DM}^{iner} = 0$. This means that the PGB-test mass displacement is the largest possible one, but that at the same time the differential displacement is not affected by this large value. In other words, in such a configuration the simulator can be used at the same time to check the level of violation of the requirements on the test masses common mode displacement in case of non drag free mode, and at the same time it can be used to detect the EP violating signal.

The Post-Processing module provides the time histories of the satellite position, velocity and acceleration in both the IRF and LVLH reference frames. It also provides the s/c-PGB and the PGB-test masses displacement, velocity and acceleration in both the IRF and LVLH reference frames, thus removing the high frequency components, which would make figures of BF time histories almost useless.

The following pictures show the time histories of the TMe common mode displacement along the three axes of the LVLH reference frame, as computed from the post-processing module.

Figure 4-5 shows the displacement of the outer test mass w.r.t. the PGB along X_{LVLH}: the maximum displacement (some tens of microns) is by far smaller than the gap between the science capacitance plate and the inner surface of the outer proof body (2.5 mm). While in this simulation the only difference of proof masses displacement is due to the EP violating signal and to gravity gradient (the differential displacement due to EP violation is Δx_{EP} = $F_{EP} \times (T_{diff})^2 / (4 \times m_{TM} \times \pi^2) \cong 0.5$ pm), in true life a fraction χ_{CMRRxy} = 10^{-5} of the observed common mode displacement is detected as differential displacement.

Figure 4-5 shows also that there is an offset on the X_{LVLH} displacement, whose value is 1 micron, which means 10 pm of differential displacement with the same frequency and phase of the EP signal: the necessity of the DFC for the compensation of the orbital component (in the IRF) of the non gravitational acceleration is here clearly stated. The larger displacement of the proof mass, i.e. the oscillation with amplitude of about 5 microns, generates (through χ_{CMRRxy} = 10^{-5}) a differential displacement which is about 2 orders of magnitude bigger than Δx_{EP}. Also this term benefits from the action of the DFC, since the drag at orbit frequency in the IRF, i.e. the main drag component, shall not contribute to the orbit frequency term of non-gravitational acceleration in the LVLH reference frame. This differential displacement, anyway, has not the same frequency of the EP violating signal and does not affect the science performance of the experiment.

Figure 4-6 shows the displacement of the outer test mass w.r.t. the PGB along Y_{LVLH}: the maximum displacement (one hundred of microns) is smaller than the gap between the science capacitance plate and the inner surface of the outer proof body (2.5 mm). Moreover, the largest part of this displacement is an offset, i.e. it is due to the orbital term (in the IRF) of the non-gravitational forces acting on the spacecraft: the presence of the DFC would reduce this displacement to about 30 microns. In this not realistic situation (absence of DFC) it is anyway demonstrated that the gap of the science capacitance read-out is not saturated. The offset along Y_{LVLH}, when "converted" into differential displacement through χ_{CMRRxy}, provides a ΔY_{LVLH} = 500 pm, i.e. a huge displacement having only a phase difference of 90° w.r.t. the EP violating signal. Again, the usefulness of the DFC is transparent and underlined.
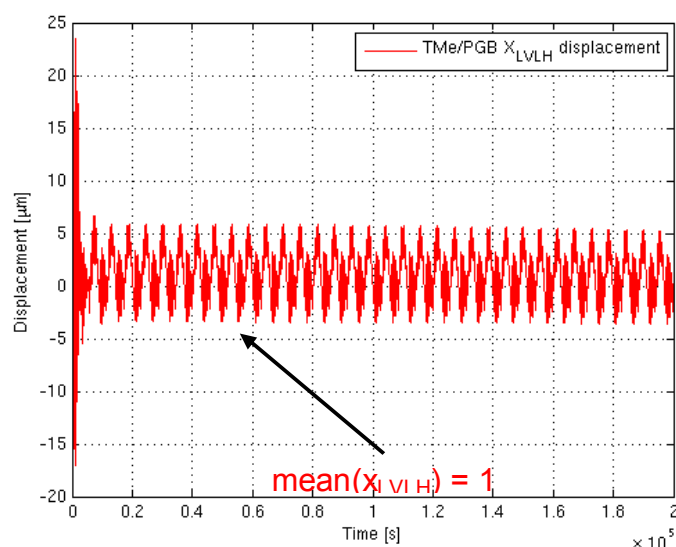
M032-EN

100181547K-EN

Figure 4-5: TMe-PGB displacement along the X_{LVLH} axis

Part of the initial transient has been removed from the picture. The displacement along X_{LVLH} is not a problem from the point of view of the gap of the science capacitance plates. The offset (mean value) of the displacement, which is about 1 micron, has the same signature of the EP violating signal. In real life, without the Drag Free control, the fraction of common mode offset along X_{LVLH} transformed into differential mode due to the imperfect CMRR ($\chi_{CMRRxy} = 10^{-5}$, i.e. not zero) of the mechanical balance, would completely mask the EP violating signal, being about 20 times greater than Δx_{EP}.
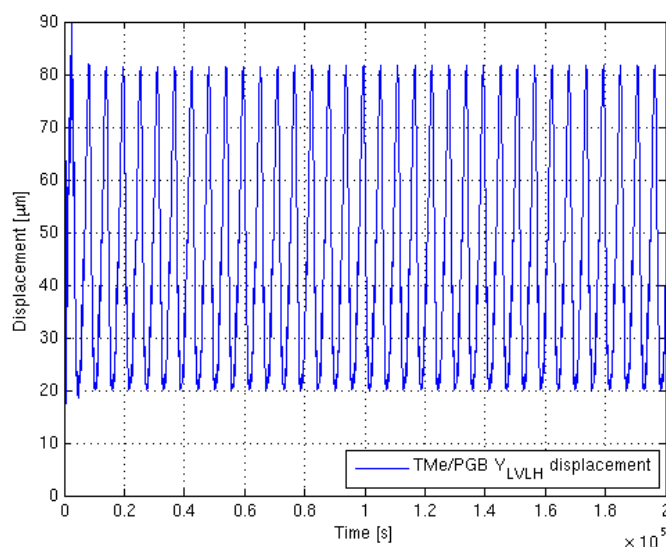

Figure 4-6: TMe-PGB displacement along the Y_{LVLH} axis

Part of the initial transient has been removed from the picture. The displacement along Y_{LVLH} is not a problem from the point of view of the gap of the science capacitance plates. The offset (mean value) of the displacement, which is about 1 micron, has the same signature of the EP violating signal. In real life, without the Drag Free control, the fraction of common mode offset along X_{LVLH} transformed into differential mode due to the imperfect CMRR ($\chi_{CMRRxy} = 10^{-5}$, i.e. not zero) of the mechanical balance, would completely mask the EP violating signal.
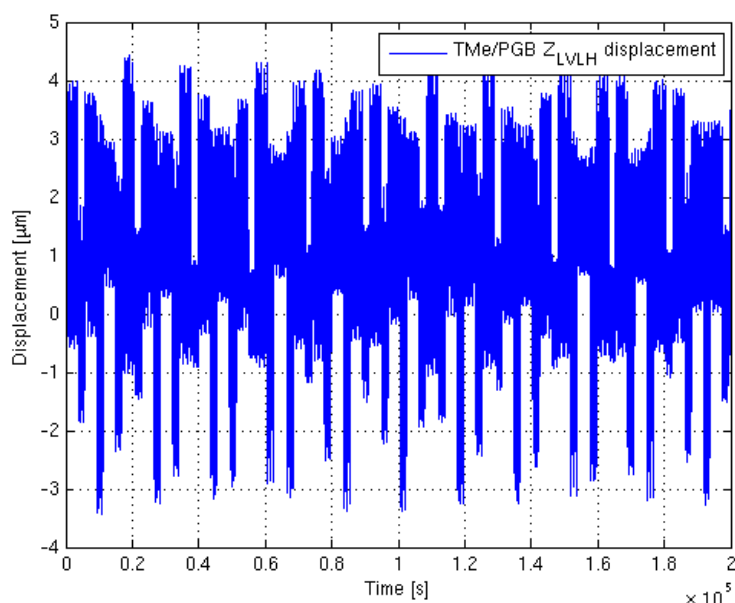
Figure 4-7: TMe-PGB displacement along the Y_{LVLH} axis

Part of the initial transient has been removed from the picture. The displacement along Y_{LVLH} is not a problem from the point of view of the gap of the science capacitance plates. The offset (mean value) of the displacement, which is about 1 micron, has the same signature of the EP violating signal. In real life, without the Drag Free control, the fraction of common mode offset along X_{LVLH} transformed into differential mode due to the imperfect CMRR (χ_{CMRRxy} = 10^{-5}, i.e. not zero) of the mechanical balance, would completely mask the EP violating signal.

Figure 4-7 shows the displacement of the outer test mass w.r.t. the PGB along Z_{LVLH}: the maximum displacement (about 5 microns) is smaller than the gap (2.5 ÷ 5 mm) of the capacitance sensors devoted to measure the proof masses displacement along the symmetry axis. In true life, the offset along Z_{LVLH}, which is about 1 micron, when "converted" into differential displacement through χ_{CMRRz} = 2·10^{-2}, provides a ΔZ_{LVLH} = 20 nm. This differential displacement along the symmetry axis, due to the gravity gradient tensor, gives rise to a differential acceleration in the test masses equatorial plane, at a frequency that is two times the orbit one (w.r.t. IRF). The requirement on the test masses differential displacement along the symmetry axis at the orbit frequency (w.r.t. IRF) is Δz^* = 0.5 nm. The maximum displacement along the symmetry axis is about 200·Δz^*. The DFC is in charge of reducing by a factor 500 the non-gravitational forces acting at the orbit frequency along the satellite spin axis: it is transparent that taking into account the DFC compensation, the differential displacement along Z_{LVLH} becomes smaller and smaller than Δz^*. The science target of being capable of measuring η=10^{-17} requires the DFC compensating action on both the orbit plane and the symmetry axis.

M032-EN

100181547K-EN

4.4 Differential mode motion of the test masses

The test masses differential displacement due only to the EP violating signal is Δx_{EP} = $a_{EP} \times (T_{diff})^2/(4 \times \pi^2)$ = 0.531936 pm (this value is obtained by using the same parameters feeding the simulator, i.e. T_{diff} = 500 s, a_{EP} = 8.4·10^{-17} m/s^2). The science read-out does not provide directly the displacement due to the EP violation only, but the overall differential displacement, which takes into account also the gravity gradient contribution. The overall expected differential displacement along X_{LVLH} is in fact:

$$\Delta x_{LVLH} = \frac{F_{EP}}{m_{TM} \cdot \left(\omega_{DM}^2 - 3 \cdot \frac{GM_\oplus}{(R_\oplus + h)^3} \right)} = 5.4449 \cdot 10^{-13} \, m$$

The time histories of the test masses differential displacement w.r.t. the IRF (after synchronous demodulation at the spin frequency) shown in Figure 4-8, highlight the orbit frequency of the expected signal. The EP violating signal is a rotating vector (at orbit frequency) w.r.t. IRF, so that X_{IRF} and Y_{IRF} are out of phase of 90°: the time delay between a maximum for the X_{IRF} component and the following Y_{IRF} one is about 1425 s (one quarter of the orbital period), as shown in Figure 4-8.
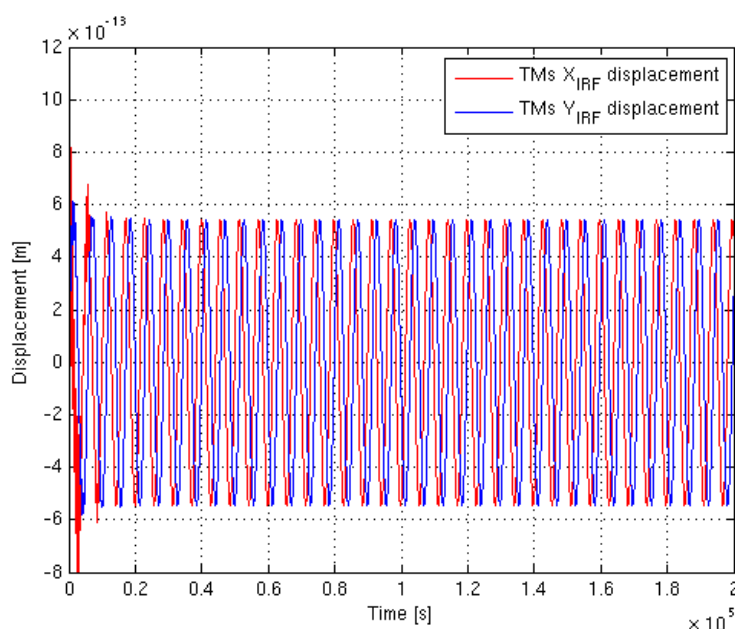

Figure 4-8: Test mass differential displacement w.r.t. the IRF. The signal signature at orbit frequency is apparent: the oscillation period of the signal is the orbit one, and the time span between a maximum for the X_{IRF} component and the following Y_{IRF} one is about 1425 s (one quarter of the orbital period).

The test masses differential displacements have to be observed in the LVLH frame in order to clear understand the test bodies' behavior and to validate the simulator (at lhe level of pm!). At first, the ΔX_{LVLH} and ΔY_{LVLH} differential displacements can be plotted in the same figure, to check their values w.r.t. the expected ones. Since the $CMRR_{xy}$ in this science performance simulation is 0, and there are not differential forces acting on the test masses along Y_{LVLH}, the expected test masses differential displacement along Y_{LVLH} is $\Delta Y_{LVLH} = 0$. Figure 4-9 shows the perfect match between the predicted differential displacements and the measured ones (accuracy is better than 1 femtometer): it has to be noticed that the gravity gradient contribution to ΔX_{LVLH} is correctly taken into account by the GG simulator.
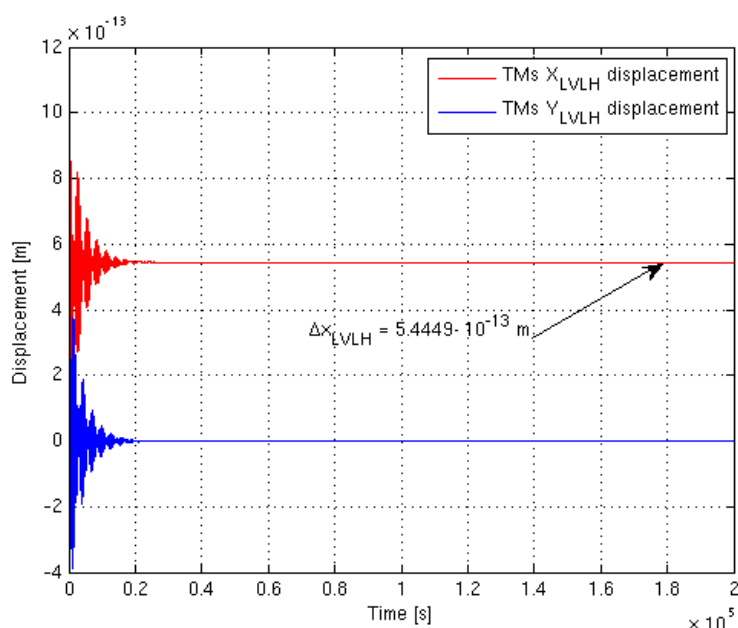

Figure 4-9: Test masses differential displacements in the LVLH frame. The measured ΔX_{LVLH} and ΔY_{LVLH} differential displacements match the predicted values with accuracy better than the femtometer. the gravity gradient contribution to ΔX_{LVLH} is correctly taken into account by the GG simulator.

The above describes results show a perfect match of the simulator vs. the expected results in the boundary conditions selected for this validating simulation. The switch-on of the imperfections, noises and of all the spurious effects, which can affect the experiments, shall be carried out with particular care, in a step by step approach, in order to check each contribution w.r.t. the overall science performance and w.r.t. the budgeted error.

4.5 Dynamic range of the simulator

The first version of the GG simulator was essentially devoted to check the experiment performance taking into account the supercritical rotation (i.e. PGB and test masses whirling motion, and whirl motion control) in the 3-dimensional space, a good model of sensors and actuators, the EP violating signal, and an ad hoc implemented environment. The GG orbit did not exist, i.e. Earth gravity field (and also gravity gradient) was not implemented in the simulator. For this reason the drag was introduced as a force with a DC term and two sinusoidal components at the nominal orbit period and at nominal half orbit period w.r.t. the IRF. At the initial time t_0, the GG satellite was coincident with the IRF origin.

The introduction of the Earth gravity field (and of gravity gradient), i.e. of the GG satellite orbit, in the simulator was not cost free. A huge dynamical range has now to be covered: from half a pico-meter differential displacement of the test masses with some significant decimal digits ($\leq 10^{-14}$ m), to the orbital radius of the satellite around the Earth ($\approx 10^7$ m). The dynamics range required to the default implementation of the DCAP software package is so $\geq 10^{21}$ m, which is beyond the double precision capability.

It has been verified that the double precision is still useful when the effort of the simulation is focused on the DFC and or whirl control performance, i.e. if it is not required to explore the test mass behaviour at the sub nano-meter level.

When the simulations are carried out in order to explore the GG mission science performance, it is required to run the simulator in quadruple machine precision. This requirement has a huge cost in terms of the CPU time: the simulator speed slows down by a factor ≈ 20 vs. the double precision run. A quadruple precision run on a Dual Xeon @3.4 GHz has almost the real time speed: the simulation of a time span of $2 \cdot 10^5$ s requires 205704 s of real CPU time.

The simulation results presented in Section 4 above have been carried out by a quadruple precision run of the GG simulator.

5. CONCLUSIONS

The development of the GG simulator is on going. In particular, the current activity is focused on the integration of the DFC and PGB whirl motion control as described in [RD 16]. This integration needs a particular care due to the necessity of running the added code in quadruple precision in case of science performance simulations.

The other foreseen development of the simulator aims to:

- Including a fine model of the selected DFC actuators

- Updating the test masses properties (inertia, magnetic, thermal) after final the selection of the materials

- Updating the modeling of the science capacitance-read-out sensor according to the final specific design for the space experiment

- Updating the capability of introducing CMRR degradation due to mechanical unbalancing (stiffness variation vs. temperature, etc.)

- Updating of the disturbing terms depending on the test masses material choices

- Consolidating the Post-Processing module.

The current version of the GG simulator is capable to explore the sub picometer world while the satellite is orbiting at an altitude of about 7000 km. This is an astonishing capability, due to the huge dynamics range ($\geq 10^{21}$ m) required to the simulating tool. The simulator is now already capable to extract the EP violating signal with $\eta = 10^{-17}$ taking into account:

- Earth gravity field and gravity gradient

- Non-gravitational forces acting on the satellite surface due to atmospheric drag, solar radiation pressure and Earth albedo

- EP violating signal

- PGB and test masses supercritical rotation with whirl motion due to the mechanical suspension dissipation

- PGB and test masses whirling motion control by means of capacitance actuators co-rotating with the satellite

- Science capacitance read-out.

The current available simulator is by far more mature than any usual Phase A simulator, due to the previous experience on the GG project and the GOCE End-to-End simulator heritage. This powerful tool shall support the GG science team for the entire duration of the Phase A study for the design phase, as a means for determining the achievable mission performance, and, consequently, trade off implementation options. In this way, specifications for all system elements can be derived, consistent with the overall goal and mutually balanced in view of the phases B/C/D. Its Post-Processing module shall suggest/support realistic procedures for scientific data reduction, based on fully representative 'raw' data. In future, during the verification phase, it shall be used as a means to establish the expected system performance,

given the measured performance of all elements, tested separately and together, as far as viable.

END OF DOCUMENT

M032-EN

100181547K-EN